JOURNAL OF Materials CHEMISTRY

Preparation of $LiCoO_2$ and $LiCo_{1-x}Fe_xO_2$ using hydrothermal reactions†

Mitsuharu Tabuchi,*[a] Kazuaki Ado,[a] Hironori Kobayashi,[a] Hikari Sakaebe,[a] Hiroyuki Kageyama,[a] Christian Masquelier,[b] Masao Yonemura,[c] Atsushi Hirano[c] and Ryoji Kanno[c]

[a]*Osaka National Research Institute, 1-8-31 Midorigaoka, Ikeda, Osaka, 563-8577, Japan*
[b]*Universite de Paris-X I, Orsay Laboratoire de Chimie des Solides, Batiment 414-91405, Orsay, Cedex, France*
[c]*Faculty of Science, Kobe University, Rokkoudai, Nada, Kobe, Hyogo, 657, Japan*

Received 13th May 1998, Accepted 29th July 1998

Iron doped/undoped $LiCoO_2$ powders could be obtained from hydrothermal reactions of either Fe^{3+} or Co^{3+} containing co-precipitates or a $CoCl_2$–NaOH–$NaClO_3$ (oxidant) mixture with an excess amount of $LiOH{\cdot}H_2O$ at 220 °C for 8–48 h. The $LiFe_xCo_{1-x}O_2$ solid solution maintained a layered rock-salt structure until $x=0.25$. ^{57}Fe Mössbauer and Co K-edge XANES spectra and magnetic susceptibility data reveal that iron and cobalt in the solid solution are in high-spin Fe^{3+} ($S=5/2$) and low-spin Co^{3+} ($S=0$) configurations.

Introduction

Lithium transition metal oxides with α-$NaFeO_2$ type (layered rock salt) structure such as $LiCoO_2$ and $LiNiO_2$ are attractive cathode materials for rechargeable lithium batteries. However, both cobalt and nickel have been considered as 'rare metals' and new cathode material containing Fe will be needed for large-scale rechargeable lithium batteries applicable to electrical vehicles, *etc.* Although lithium ferrite, $LiFeO_2$ has been regarded as a promising cathode material, neither Li extraction nor insertion have been reported for α, β and γ forms obtained by solid state reaction of α-Fe_2O_3 and Li_2CO_3.[1] Reimers *et al.* prepared $LiFe_xNi_{1-x}O_2$ by a solid state reaction, in which Fe could be incorporated into the layered structure with $x=0$–0.2 and charge and discharge capacities decreased with increasing Fe content.[2] On the other hand, electrochemically-active $LiFeO_2$ with corrugate layer[3] and Goethite type[4] structures were synthesized by an ion-exchange reaction using γ-FeOOH and α-FeOOH as host materials, respectively, indicating that the soft-chemical synthesis is suitable for isolating new cathode materials because of the mild preparation temperature. The hydrothermal preparation method is a soft-chemical route, and $LiMO_2$ (M = Fe, Mn or Co) could be obtained by hydrothermal treatment below 250 °C.[5–7] Recently, metastable $LiFeO_2$ with a layered rock salt structure (layered-$LiFeO_2$) could be obtained hydrothermally at 220 °C from Fe^{3+} sources such as α-FeOOH into excess amounts of LiOH–KOH or LiOH–NaOH mixed-alkaline solutions.[8] If the hydrothermal process could be used for Fe doping to $LiCoO_2$, the solubility limit would be extended to higher Fe content due to the mild preparation conditions.

Experimental

$CoCl_2{\cdot}6H_2O$ (purity 99.0%, Kishida Chem.), $Co(NO_3)_2{\cdot}6H_2O$ (reagent grade, Kanto Chem.), $Fe(NO_3)_3{\cdot}9H_2O$ (purity 99.0%, Wako Pure Chem.), 36% hydrochloric acid (reagent grade, Ishizu Seiyaku), $LiOH{\cdot}H_2O$ (purity 98.0%, Wako Pure Chem.), NaOH (purity 96.0%, Wako Pure Chem.) and $NaClO_3$ (purity 98.0%, Wako Pure Chem.) were used as starting materials. Two different starting mixtures were used for hydrothermal preparations of $LiCoO_2$ (samples A and B). For sample A, $CoCl_2{\cdot}6H_2O$ (5.94 g) was dissolved in distilled water (90 ml) in a beaker, and then concentrated HCl (2 ml), $NaClO_3$ (oxidant, 2.0 g), $LiOH{\cdot}H_2O$ (12.0 g) and NaOH (84 g) were added to the aqueous solution. For sample B, CoOOH (2.7 g) and $LiOH{\cdot}H_2O$ (50 g) were used as reactants with distilled water (100 ml). CoOOH was obtained by bubbling air through the $Co(OH)_2$ precipitate which was made by adding a 4.5 M NaOH solution (400 ml) dropwise to a 1 M $Co(NO_3)_2$ solution (400 ml). For Fe doped samples (samples C–G), a 1 M $(1-x)Co(NO_3)_2$–$xFe(NO_3)_3$ mixed aqueous solution was selected, instead of a 1 M $Co(NO_3)_2$ solution. All reactants were hydrothermally treated at 220 °C for 5–48 h in autoclaves (Sakashita Chem.), washed repeatedly with distilled water, filtered and dried at 100 °C to eliminate residual alkali and salts from the products. For comparison, α-$NaFeO_2$, α-$LiFeO_2$ and layered-$LiFeO_2$ (sample H) were prepared from α-FeOOH–NaOH,[5] α-FeOOH–$LiOH{\cdot}H_2O$[5] and α-FeOOH–$LiOH{\cdot}H_2O$–KOH[8] mixtures by the hydrothermal reaction at 220 °C for 8 h, respectively.

The samples obtained were identified by X-ray diffractometry (XRD, Rigaku Rotaflex/RINT) using monochromatized Cu-Kα radiation. Si powders were used to calibrate 2θ angles (>10°). The XRD data were collected for 10 s at each 0.02° step over a 2θ range from 10 to 120° for Rietveld analysis. Reflection positions and intensities were calculated for both Cu-Kα_1 and Cu-Kα_2 reflections. A pseudo-Voigt profile function was used. The computer program, RIETAN97 Beta[9] was used for Rietveld analysis. Calculated patterns were constructed using a layered rock salt ($R\bar{3}m$, α-$NaFeO_2$ type structure) model with ideal cation ordering and a cubic rock salt ($Fm\bar{3}m$, α-$LiFeO_2$ type structure) one. Thermal parameters of cation and anions were fixed at appropriate values between 0.4 and 1.0 $Å^2$ using previous neutron and X-ray diffraction analysis data.[2,10–13]

The cation contents in the obtained solids were determined by inductive coupled plasma (ICP) emission (Li, Co and Fe) and atomic absorption spectroscopy (Na and K).

The Co K-edge XANES spectra of the samples were measured by transmission mode with a laboratory type X-ray spectrometer,[14] EXAC-820 (Technos) at 293 K. The X-ray generator with a Mo rotating anode and a LaB_6 cathode was operated with a voltage of 20 kV and a current of 200 mA.

†Basis of the presentation given at Materials Chemistry Discussion No. 1, 24–26 September 1998, ICMCB, University of Bordeaux, France.

The incident X-ray beam was monochromatized with a Ge(400) Johansson curved crystal. It is reported that resolution of spectra in this system is comparable to that in a conventional beam line of a synchrotron radiation facility.[14] The intensity of the X-ray beam was measured by a sealed proportional counter filled with 25% Ar and 75% N_2 gases for the incident X-rays and by a solid state detector for the transmitted X-rays. The monochromator angle was calibrated with a characteristic Mo X-ray line for each machine time. The Co powders, cobalt(II) acetylacetonate dihydrate, cobalt(III) acetylacetonate and $LaCoO_3$, were used as reference samples.

^{57}Fe Mössbauer spectra were taken at room temperature (FGX-100, Topologic Systems). α-Fe was used for velocity calibration. Observed spectra were fitted by absorption peaks of Lorentzian line shape.

The magnetization was measured between 83 and 300 K, with a magnetic balance using the Faraday method (MB-3, Shimadzu) between 1.8 and 12.5 kOe. Since small spontaneous magnetization (M_s) was observed, we subtracted the contribution of M_s from the total magnetization value at each magnetic field between 1.8 and 12.5 kOe when obtaining magnetic susceptibility data. Temperature and magnetic susceptibility data were calibrated using $(NH_4)_2Mn(SO_4)_3 \cdot 6H_2O$ as a standard.

Results and discussion

The layered rock salt model ($R\bar{3}m$) of HT-$LiCoO_2$[11] with ideal cation ordering could fit both XRD patterns of samples A and B (Fig. 1 and Table 1). Each XRD peak for sample B was slightly broader than that for sample A due to the low crystallinity, because TEM observations [Fig. 2(a) and (b)] showed a smaller particle size (<0.5 μm) of sample B than that (hexagonal platelet-like crystal, >1 μm) of sample A. Uniform particle shape of each sample suggests that $LiCoO_2$ precipitated from the solution. The XRD patterns for iron-doped $LiFe_xCo_{1-x}O_2$ (samples C–F) of up to $x=0.4$ in the nominal formula (Fig. 3) were similar to that of the undoped one (sample B), α-$LiFeO_2$ with a cubic rock salt structure coexists with the rhombohedral phase ($R\bar{3}m$) in the 50% Fe doped sample (sample G). This means that the solubility limit

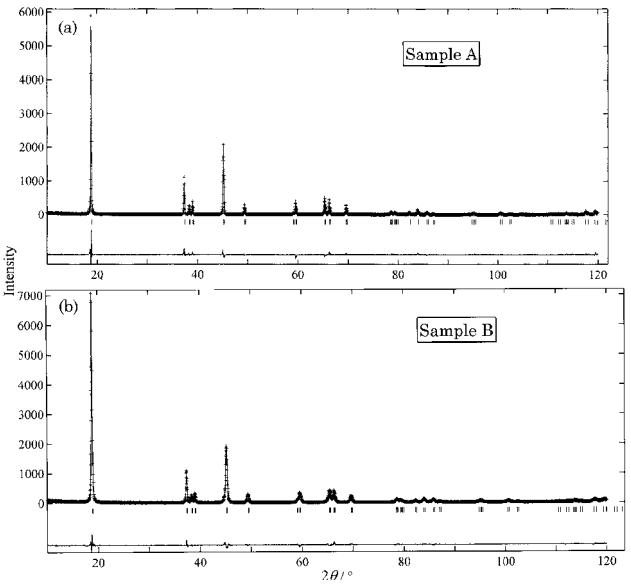

Fig. 1 Observed (+) and calculated (solid line) X-ray diffraction patterns for products obtained by hydrothermal reaction of $CoCl_2$–$LiOH \cdot H_2O$–$NaClO_3$ (sample A) (a) and CoOOH–$LiOH \cdot H_2O$ (sample B) (b) mixtures at 220 °C. Each calculated pattern was constructed from a layered rock salt model ($R\bar{3}m$).

Table 1 X-Ray Rietveld refinement results for samples A and B using a layered rock-salt model ($R3m$)

Atom	Site	g	x	y	z	B/Å^2
Sample A						
Li	3*a*	1	0	0	0	1.0
Co	3*b*	1	0	0	0.5	0.4
O	6*c*	1	0	0	0.2386(16)	0.6
$a=2.81789(6)$ Å, $c=14.0582(3)$ Å, $R_{wp}=23.98$, $R_p=17.12$, $S=1.36$, $R_I=7.56$, $R_F=5.11$.						
Sample B						
Li	3*a*	1	0	0	0	1.0
Co	3*b*	1	0	0	0.5	0.4
O	6*c*	1	0	0	0.2390(10)	0.6
$a=2.81800(9)$ Å, $c=14.0640(4)$ Å, $R_{wp}=14.94$, $R_p=10.14$, $S=1.20$, $R_I=2.79$, $R_F=2.21$.						

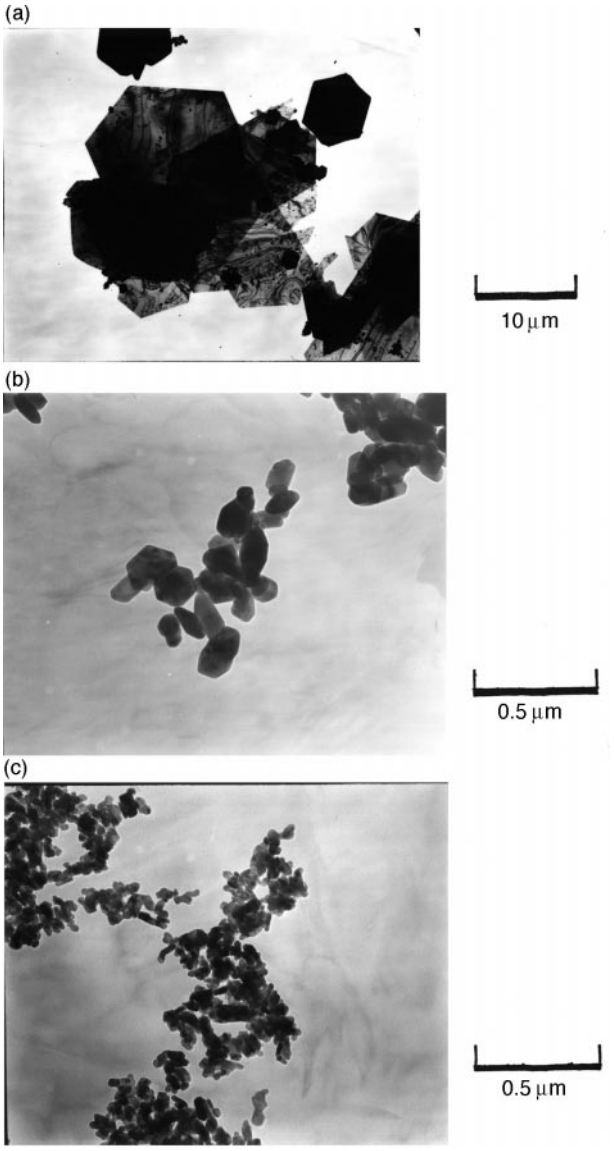

Fig. 2 TEM photographs for samples A (a), B (b) and D (c).

of $LiFe_xCo_{1-x}O_2$ is less than $x=0.4$. The XRD peak broadening by Fe doping may be attributed to the suppression of grain growth, because sample D consisted of smaller particle sizes (≈0.1 μm) than those for the undoped sample B (Fig. 2). The change in lattice parameters (Fig. 4) as a function of Fe content (x) and chemical analysis data of Li, Co, Fe and Na (Table 2) also support the formation of $LiFe_xCo_{1-x}O_2$ below $x=0.4$. The sum of Fe and Co contents for the solid solutions

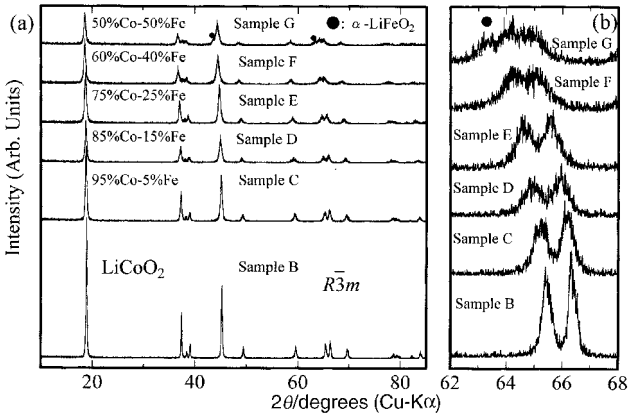

Fig. 3 XRD patterns of products obtained by hydrothermal reaction of lithium hydroxide and oxidized Fe–Co co-precipitates at 220 °C (a) and a close up of the region around 66° (b). Initial molar fractions of Fe and Co are indicated on the figure. Hydrothermal reaction times are selected to be 8–12 h for samples A–F and 48 h for sample G.

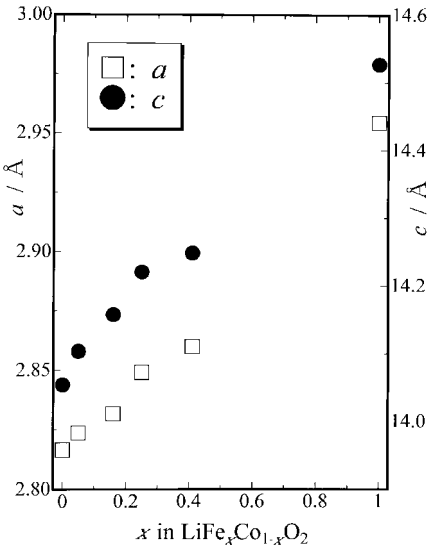

Fig. 4 Change in lattice parameters of the hexagonal unit cell as a function of Fe content (x) in $LiFe_xCo_{1-x}O_2$. The values of layered $LiFeO_2$ (sample H) obtained by mixed-alkaline hydrothermal reaction were used for comparison.

is slightly lower than the expected value of $LiFe_xCo_{1-x}O_2$. The difference in cation contents may be attributed to the incorporation of other ions or molecules such as H^+, H_3O^+ and/or occluded water to the iron-doped samples, because particle size of these samples is much smaller (>1 μm) than those of the two end-members, samples A and H. Although X-ray Rietveld analysis for each XRD pattern for samples C–E revealed that they could be fitted to a layered rock salt model ($R\bar{3}m$) without cation disordering, the XRD pattern of sample F was well fitted to the mixture of 80% layered and 20% cubic rock salt models (Fig. 5 and Table 3). The homogeneous $LiFe_xCo_{1-x}O_2$ solid solution was formed up to $x=0.25$ by a hydrothermal reaction.

Almost no difference in Co K-edge XANES spectra between the data for $LiCoO_2$ (samples A and B) and $LiFe_xCo_{1-x}O_2$ (samples C–E) (Fig. 6) indicate that the valence state of Co in the latter is close to the low-spin trivalent state ($S=0$) as in $LiCoO_2$.[15]

Only a doublet could be detected in the ^{57}Fe Mössbauer spectra for the samples C–E (Fig. 7) at 300 K, which is an indication of the paramagnetic state of the samples. Each doublet could be fitted by at least two doublets with a similar isomer shift (IS) and different quadrupole splitting (QS) values (Table 4), indicating the presence of the QS distribution. The

Table 3 X-Ray Rietveld refinement results for samples C–F using a layered rock-salt model ($R\bar{3}m$)

Atom	Site	g	x	y	z	B/Å^2
Sample C						
Li	3*a*	1	0	0	0	1.0
Co/Fe[a]	3*b*	1	0	0	0.5	0.4
O	6*c*	1	0	0	0.2400(11)	0.6
$a=2.82071(9)$ Å, $c=14.0922(7)$ Å, $R_{wp}=10.99$, $R_p=8.04$, $S=1.44$, $R_I=1.90$, $R_F=1.58$.						
Sample D						
Li	3*a*	1	0	0	0	1.0
Co/Fe	3*b*	1	0	0	0.5	0.4
O	6*c*	1	0	0	0.2403(10)	0.6
$a=2.83469(12)$ Å, $c=14.1745(10)$ Å, $R_{wp}=11.24$, $R_p=8.06$, $S=1.26$, $R_I=2.75$, $R_F=2.07$.						
Sample E						
Li	3*a*	1	0	0	0	1.0
Co/Fe	3*b*	1	0	0	0.5	0.4
O	6*c*	1	0	0	0.2417(11)	0.6
$a=2.84567(13)$ Å, $c=14.2206(10)$ Å, $R_{wp}=10.86$, $R_p=7.99$, $S=1.46$, $R_I=2.32$, $R_F=1.26$.						
Sample F						
Li	3*a*	1	0	0	0	1.0
Co/Fe	3*b*	1	0	0	0.5	0.4
O	6*c*	1	0	0	0.2397(14)	0.6
$a=2.8587(3)$ Å, $c=14.273(2)$ Å, $R_{wp}=8.80$, $R_p=6.38$, $S=1.85$, $R_I=2.74$, $R_F=1.37$.						
Sample F [cubic rock-salt model ($Fm\bar{3}m$)]						
Li	4*a*	0.5	0	0	0	0.6
Co/Fe	4*a*	0.5	0	0	0	0.6
O	4*b*	1	0.5	0.5	0.5	0.6
$a=4.0929(10)$ Å, $R_{wp}=8.80$, $R_p=6.38$, $S=1.85$, $R_I=1.97$, $R_F=1.06$. Mass fraction of compound, rhombohedral phase:cubic phase = 0.81:0.19.						

[a]Fe and Co present in 3*b* sites.

Table 2 Chemical analysis data for $LiCo_{1-x}Fe_xO_2$ samples prepared by hydrothermal reactions compared with the ideal cation content derived from $LiCoO_2$ and $LiFeO_2$

Sample name	Li/wt%	Co/wt%	Fe/wt%	Na/wt%	K/wt%	Li/($Co_{1-x}Fe_x$)	x
Sample A	7.07(3)	58.7(6)	—	<0.01	—	1.02(1)	0.00
Sample B	6.98(5)	58.5(2)	—	<0.01	—	1.01(1)	0.00
Sample C	6.12(7)	51.9(10)	2.72(5)	<0.01	—	0.95(3)	0.05
Sample D	6.83(5)	48.6(2)	8.30(6)	<0.01	—	1.01(1)	0.16
Sample E	6.57(3)	43.5(3)	14.1(1)	<0.01	—	0.96(1)	0.25
Sample F	6.11(2)	34.8(4)	23.1(1)	<0.01	—	0.88(1)	0.41
Sample G	5.50(5)	29.7(1)	28.3(1)	<0.01	—	0.78(1)	0.50
Sample H	7.25(4)	—	58.0(3)	—	<0.01	1.01(1)	1.00
$LiCoO_2$	7.09	60.2	—	—	—	1.00	0.00
$LiFeO_2$	7.31	—	58.9	—	—	1.00	1.00

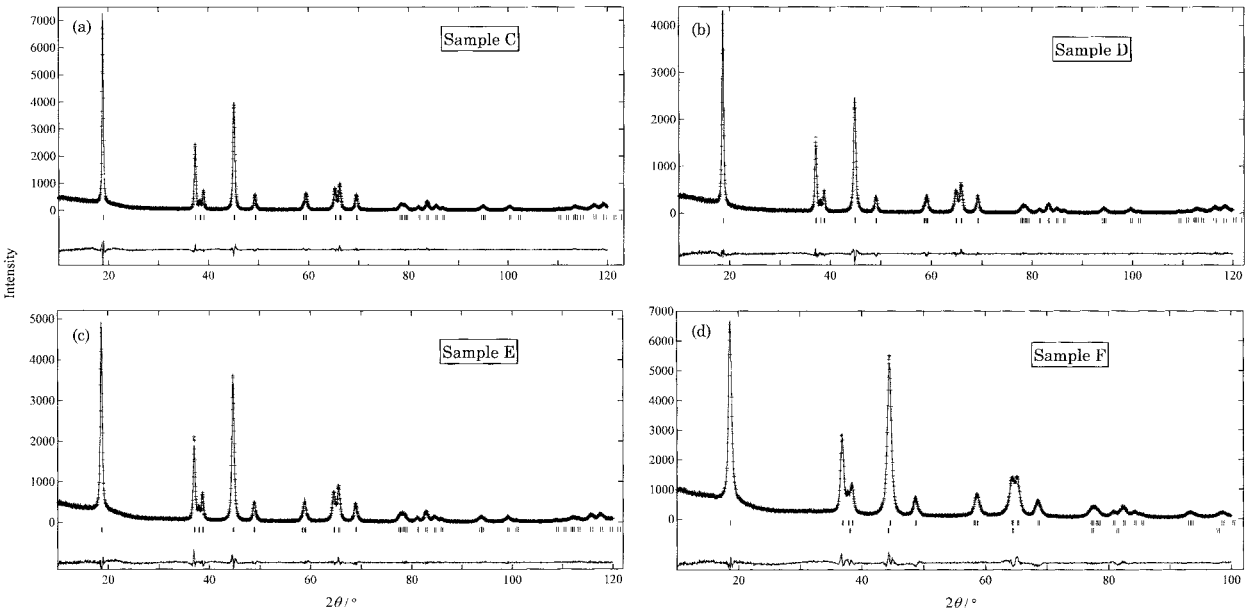

Fig. 5 Observed (+) and calculated (solid line) X-ray diffraction patterns for iron-doped samples C ($x=0.05$)–F ($x=0.41$), (a)–(d). Each calculated pattern was constructed from either a layered rock salt model ($R\bar{3}m$) or a mixture of layered and cubic rock salt models.

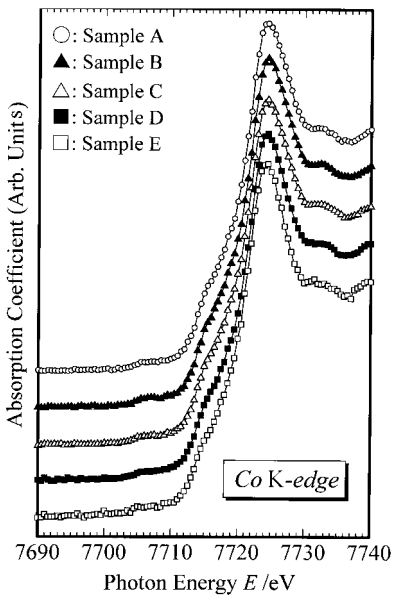

Fig. 6 Co K-edge XANES spectra for samples A–E at 293 K.

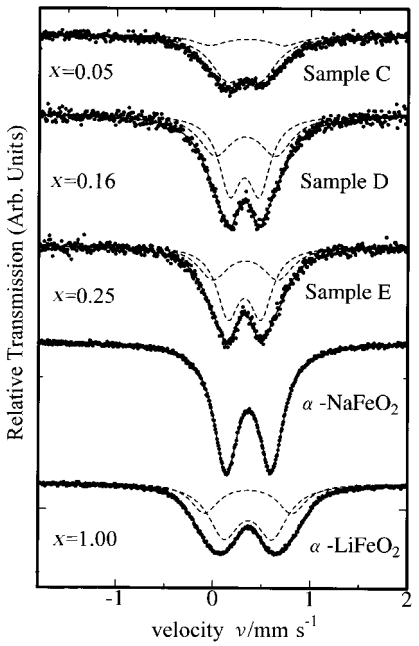

Fig. 7 ^{57}Fe Mössbauer spectra of $LiCo_{1-x}Fe_xO_2$ (samples C–E), α-$NaFeO_2$ and α-$LiFeO_2$ at 300 K. Observed (●) and calculated spectra (solid line) are shown. Each doublet for making calculated spectra was designated as a break line.

QS distribution suggests that the cation coordination state around a Fe^{3+} ion is not unique, because α-$NaFeO_2$ with a typical layered rock-salt structure gives a simple doublet (Fig. 7). However, the QS distribution was also considered for fitting the spectrum of α-$LiFeO_2$ in which Fe^{3+} and Li^+ (a diamagnetic ion) occupy octahedral sites in a random fashion. The similarity in spectra between our samples and α-$LiFeO_2$ suggests that the QS distribution for each iron-doped sample can be caused by partial occupation of iron into the diamagnetic Co layer in the layered rock-salt structure. At 5 K, the Mössbauer spectra for Fe doped $LiCoO_2$ ($x=0.16$ or 0.25) consisted of a doublet and a sextet. This result also supports the presence of two or more local coordination structures around Fe. The observed isomer shift data for these samples revealed that Fe is present in a high-spin 3+ state ($S=5/2$) as these values were close to those for α-$NaFeO_2$ and α-$LiFeO_2$ which are typical high-spin Fe^{3+} compounds.[16,17] The Co K-edge XANES and ^{57}Fe Mössbauer spectra indicate the trivalent state of the transition metals in the $LiFe_xCo_{1-x}O_2$ solid solution.

The magnetic field dependence of magnetization (M) at 295 and 83 K for samples A–E gives positive magnetic susceptibility values and no spontaneous magnetization, which means that M/H is equal to the magnetic susceptibility value. The occurrence of positive magnetization values for both $LiCoO_2$ samples is due to the presence of paramagnetic ions such as high-spin Co^{2+} ($S=3/2$) and/or high-spin Co^{3+} ($S=2$), because $LiCoO_2$ with only low-spin Co^{3+} ion ($S=0$) is expected to be an diamagnetic compound.[15] The temperature dependence of inverse molar susceptibility (χ_m^{-1}, Fig. 8) reveals a Curie–Weiss paramagnetic behavior ($\chi_m^{-1}=(T-\theta)/C$; (θ=Weiss temperature, C=Curie constant) for

Table 4 Mössbauer parameters for $LiCo_{1-x}Fe_xO_2$ samples with α-$NaFeO_2$ at 300 K

Sample	x	Component	Area (%)	IS/mm s^{-1}	QS/mm s^{-1}	Γ/mm s^{-1}
Sample C	0.05	I	79.1	+0.303(3)	0.35(1)	0.41(2)
		II	20.9	+0.34(1)	0.77(4)	0.41(2)
Sample D	0.16	I	55.6	+0.316(2)	0.30(1)	0.27(2)
		II	44.4	+0.325(3)	0.62(4)	0.41(2)
Sample E	0.25	I	59.9	+0.319(2)	0.34(1)	0.28(1)
		II	40.1	+0.326(3)	0.67(4)	0.38(2)
α-$NaFeO_2$	—	I	100.0	+0.3662(3)	0.4680(5)	0.3000(8)
α-$LiFeO_2$	1.00	I	65.3	+0.3643(7)	0.495(6)	0.384(6)
		II	34.7	+0.364(1)	0.899(8)	0.348(9)

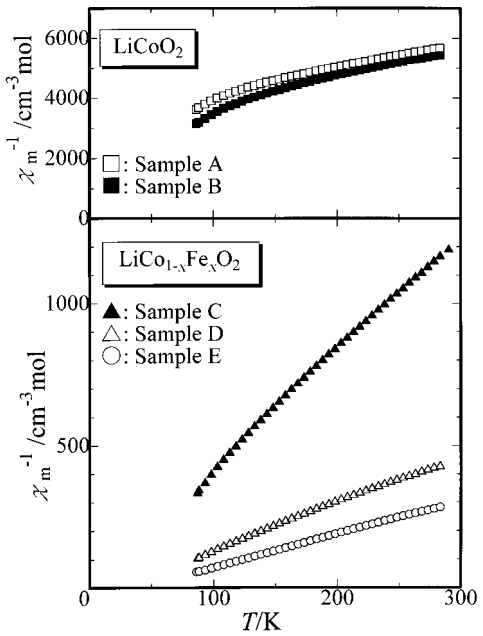

Fig. 8 Temperature dependence of the inverse molar susceptibility (χ_m^{-1}) for samples A–E.

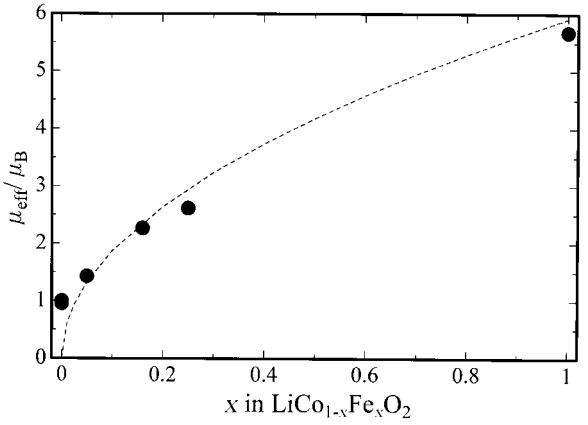

Fig. 9 Fe content dependence of effective magnetic moment (μ_{eff}) for samples A–E. Broken line indicates the calculated curve using the equation, $\mu_{eff}^2 = x\mu_{eff,\,Fe}^2 + (1-x)\,\mu_{eff,\,Co}^2$, assuming that only high-spin Fe^{3+} ($S=5/2$, spin only value of $\mu_{eff}=\sqrt{35}\,\mu_B$) and low-spin Co^{3+} ($S=0$, spin only value of $\mu_{eff}=0\,\mu_B$) exist in the $LiFe_xCo_{1-x}O_2$ solid solution.

samples A–E above 120 K. Changes in the effective magnetic moment (μ_{eff}) with increasing Fe content (Table 5 and Fig. 9) could be explained by comparing with the calculated curve derived from the assumption that only Fe^{3+} ($S=5/2$) and Co^{3+} ($S=0$) are present in $LiFe_xCo_{1-x}O_2$ (see caption of Fig. 9). Concerning the valence states of Fe and Co ions, the magnetic susceptibility data confirm the results from Co K-edge XANES and ^{57}Fe Mössbauer spectra. θ values for Fe-doped samples change gradually from negative to positive with increasing x, indicating that ferromagnetic interactions are predominant in total magnetic interactions in samples with high Fe doping (samples D and E), because θ would remain negative if the amount of ferrimagnetic impurities, $LiFe_5O_8$ and/or γ-Fe_2O_3, increased with increasing Fe content. SQUID and ^{57}Fe Mössbauer spectroscopic measurements below 100 K are now in progress to confirm whether magnetic ordering occurs or not. An electrochemical test using a Li coin-type cell will be performed.

Table 5 Paramagnetic parameters of $LiCo_{1-x}Fe_xO_2$ using hydrothermal reactions

Sample	x	μ_{eff}/μ_B	θ/K
Sample A	0.00	0.999(5)	−428
Sample B	0.00	0.955(6)	−343
Sample C	0.05	1.430(3)	−16
Sample D	0.16	2.269(7)	+5
Sample E	0.25	2.615(4)	+37

Conclusion

Iron doped/undoped $LiCoO_2$ can be precipitated from solutions by hydrothermal reactions. Although high crystallinity $LiCoO_2$ with large particle sizes could be obtained from a $CoCl_2$–LiOH–NaOH–$NaClO_3$ mixture, Fe doped $LiCoO_2$ was formed from a mixture of air-oxidized Co–Fe co-precipitates and LiOH. The Fe content could be adjusted by initial Co–Fe atomic ratios. High-spin Fe^{3+} and low-spin Co^{3+} are mainly present in the solid solution. These hydrothermal reactions may be a promising method for $LiCoO_2$ based solid solution for lithium-ion batteries.

M. T. expresses his gratitude to Kiyoshi Fukai and Yoshiyuki Kira of Sakai Chemical for their fruitful advice and his hearty thanks to Mr. M. Wakita and Professor S. Nasu of Osaka University for their Mössbauer measurements at 5 K and fruitful discussions.

References

1 J. C. Anderson and M. Schieber, *J. Phys. Chem. Solids*, 1964, **25**, 961.
2 J. N. Reimers, E. Rossen, C. D. Jones and J. R. Dahn, *Solid State Ionics*, 1993, **61**, 335.
3 R. Kanno, T. Shirane, Y. Kawamoto, Y. Takeda, M. Takano, M. Ohashi and Y. Yamaguchi, *J. Electrochem. Soc.*, 1996, **143**, 2435.
4 Y. Sakurai, H. Arai, S. Okada and J. Yamaki, *J. Power Sources*, 1997, **68**, 711.
5 M. Tabuchi, K. Ado, H. Sakaebe, C. Masquelier, H. Kageyama and O. Nakamura, *Solid State Ionics*, 1995, **79**, 220.
6 M. Tabuchi, K. Ado, C. Masquelier, I. Matsubara, H. Sakaebe, H. Kageyama, H. Kobayashi, R. Kanno and O. Nakamura, *Solid State Ionics*, 1996, **89**, 53.

7 D. Larcher, M. R. Palacin, G. G. Amatucci and J. M. Tarascon, *J. Electrochem. Soc.*, 1997, **144**, 408.
8 K. Ado, M. Tabuchi, H. Kobayashi, O. Nakamura, Y. Inaba, R. Kanno, M. Takagi and Y. Takeda, *J. Electrochem. Soc.*, 1997, **144**, L177.
9 F. Izumi, *The Rietveld Method*, ed. R. A. Young, Oxford University Press, Oxford, 1993, ch. 13.
10 T. Shirane, R. Kanno, Y. Kawamoto, Y. Takeda, M. Takano, T. Kamiyama and F. Izumi, *Solid State Ionics*, 1995, **79**, 227.
11 R. J. Gummow, M. M. Thackeray, W. I. F. David and S. Hull, *Mater. Res. Bull.*, 1992, **27**, 327.
12 R. Kanno, H. Kubo, Y. Kawamoto, T. Kamiyama, F. Izumi, Y. Takeda and M. Takano, *J. Solid State Chem.*, 1994, **110**, 216.
13 A. Hirano, R. Kanno, Y. Kawamoto, Y. Nitta, K. Okamura, T. Kamiyama and F. Izumi, *J. Solid State Chem.*, 1997, **134**, 1.
14 K. Nishihagi, A. Kawabata and K. Taniguchi, *Jpn. J. Appl. Phys. Part 2*, 1993, **32**, 258.
15 E. Zhecheva and R. Stoyanova, *J. Solid State Chem.*, 1994, **109**, 47.
16 D. E. Cox, G. Shirane, P. A. Flinn, S. L. Ruby and W. J. Takei, *Phys. Rev.*, 1963, **132**, 1547.
17 T. Ichida, T. Shinjo and Y. Bando, *J. Phys. Soc. Jpn.*, 1970, **29**, 795.

Paper 8/05311A